



Universitat de Lleida

Document downloaded from:

<http://hdl.handle.net/10459.1/69372>

The final publication is available at:

<https://doi.org/10.1002/esp.4086>

Copyright

(c) John Wiley & Sons, 2016

**Earth Surface
Processes and Landforms**

**Application of Structure-from-Motion Photogrammetry to
river restoration**

Journal:	<i>Earth Surface Processes and Landforms</i>
Manuscript ID	ESP-16-0107.R2
Wiley - Manuscript type:	Special Issue Paper
Date Submitted by the Author:	n/a
Complete List of Authors:	Marteau, Baptiste; Northern Rivers Institute, Geography Vericat, Damià; Univeristy of Lleida, Department of Environment and Soil Sciences Gibbins, Chris; University of Aberdeen, Northern Rivers Institute, School of Geosciences Batalla, Ramon; University of Lleida, Department of Environment and Soil Sciences; Green, David; Aberdeen Institute for Coastal Science and Management (AICSM), School of Geosciences
Keywords:	Structure-from-Motion Photogrammetry, River Restoration, UAV, Digital Elevation Models, Geomorphic Change

SCHOLARONE™
Manuscripts

1

2

3

4

5

6

7

8

9

10

11

12

13

14

15

16

17

18

19

20

21

22

23

24

25

26

27

28

29

30

31

32

33

34

35

36

37

38

39

40

41

42

43

44

45

46

47

48

49

50

51

52

53

54

55

56

57

58

59

60

1

2

3

4

5

6

7

8

9

10

11

12

13

14

15

16

17

18

19

20

21

22

23

24

25

26

27

28

29

30

31

32

33

34

35

36

37

38

39

40

41

42

43

44

45

46

47

48

49

50

51

52

53

54

55

56

57

58

59

60

Application of Structure-from-Motion
photogrammetry to river restoration

Baptiste Marteau^{1,*}, Damià Vericat^{2,3}, Chris Gibbins¹, Ramon J. Batalla^{2,4}, David R. Green⁵.

¹ Northern Rivers Institute (NRI), Geosciences, University of Aberdeen (Scotland, UK)

² Fluvial Dynamics Research Group (RIUS), University of Lleida, Lleida (Catalonia, Spain)

³ Forest Technology Centre of Catalonia (CTFC), Solsona (Catalonia, Spain)

⁴ Catalan Institute for Water Research (ICRA), Girona (Catalonia, Spain)

⁵ UCEMM - Aberdeen Institute for Coastal Science and Management (AICSM), University of Aberdeen (Scotland, UK)

*Corresponding author: baptiste.marteau@abdn.ac.uk

Abstract

Structure-from-Motion (SfM) photogrammetry is now used widely to study a range of earth surface processes and landforms, and is fast becoming a core tool in fluvial geomorphology. SfM photogrammetry allows extraction of topographic information and orthophotos from aerial imagery. However, one field where it is not yet widely used is that of river restoration. The characterisation of physical habitat conditions pre- and post-restoration is critical for assessing project success, and SfM can be used easily and effectively for this purpose. In this paper we outline a workflow model for the application of SfM photogrammetry to collect topographic data, develop surface models and assess geomorphic change resulting from river restoration actions. We illustrate the application of the model to a river restoration project in the NW of England, to show how SfM techniques have been used to assess whether the project is achieving its geomorphic objectives. We outline the details of each stage of the workflow, which extend from preliminary decision-making related to the establishment of a ground control network, through fish-eye lens camera testing and calibration, to final image analysis for the creation of facies maps, the extraction of point clouds, and the development of Digital Elevation Models (DEMs) and channel roughness maps. The workflow enabled us to confidently identify geomorphic changes occurring in the river channel over time, as well as assess spatial variation in erosion and aggradation. Critical to the assessment of change was the high number of ground control points and the application of a minimum level of detection threshold used to assess uncertainties in the topographic models. We suggest that these two things are especially important for river restoration applications.

Key words: Structure-from-Motion, Photogrammetry, River Restoration, UAV, High Resolution Topography, Digital Elevation Models, Geomorphic Change.

1
2
3
4
5
6
7
8
9
10
11
12
13
14
15
16
17
18
19
20
21
22
23
24
25
26
27
28
29
30
31
32
33
34
35
36
37
38
39
40
41
42
43
44
45
46
47
48
49
50
51
52
53
54
55
56
57
58
59
60

Introduction

Developments in surveying techniques (e.g. terrestrial and airborne LiDAR) alongside the availability of improved data-processing tools (e.g. GIS and remote sensing software, open source geostatistical toolkits) have brought geomorphological science into a new era (see recent reviews by Bangen *et al.*, 2014 and Smith *et al.*, 2015). This new era is changing not only the way in which we can characterise landscapes but also how we understand the processes which shape them. The new era is particularly evident in fluvial geomorphology, where the application of newly evolving survey and processing tools has been seen as heralding-in the High Resolution Topography (HRT) revolution (as described recently by Vericat *et al.*, 2016). This revolution is greatly improving our ability to assess geomorphic change in river channels, whether in the context of human impacts or natural fluvial dynamics.

HRT was defined by Passalacqua *et al.* (2015) as topographic surveys at a minimum of the metre resolution. In fluvial geomorphology, HRT is most commonly used for: (i) landscape characterisation (e.g. topography, roughness; Heritage and Milan, 2009; Brasington *et al.*, 2012; Tamminga *et al.*, 2014; Woodget *et al.*, 2014), and/or (ii) monitoring topographic changes (e.g. quantification of the volume of sediments mobilised; Lane *et al.*, 2003). Several commonly used technologies allow the collection of HRT data (Passalacqua *et al.*, 2015), but increasing use is now being made of digital photogrammetry via Structure-from-Motion (SfM) and Multi View Stereo (MVS) techniques (hereafter together referred to as SfM, James and Robson, 2012). One of the advantages of SfM over other HRT acquisition methods is the collection of topographic information and orthophotos at multiple spatial scales (from the microhabitat or patch scale (m^2) to the scale of river reaches (tens, hundreds or even thousands of metres in length, Dietrich, 2016)), and with a resolution appropriate for many applications (e.g. topographic change detection, Wheaton *et al.*, 2010a, 2010b;

hydrodynamic modelling, Tamminga *et al.*, 2014). While the basic concepts are similar, SfM differs from traditional photogrammetry in the fact that little expertise is required, image processing and camera calibration can be fully automated and relatively few control points are required (James and Robson, 2012). SfM creates a light 3D point cloud from automatically aligned overlapping images, while the MVS algorithms then allow for the generation of a high-density 3D point cloud (detailed in James and Robson, 2012; Micheletti *et al.*, 2015; Smith *et al.*, 2015). The rapid improvement in Unmanned Aerial Vehicle (UAV) platforms is facilitating the acquisition of high quality aerial imagery from which SfM can be applied to obtain orthophotos and point clouds (e.g. Javernick *et al.*, 2014; Woodget *et al.*, 2014; Smith and Vericat, 2015).

The acquisition of HRT data is now commonplace, and as a result the HRT revolution has changed the nature of the problem faced by geomorphologists. Historically the problem was one of being able to collect sufficient data to adequately capture the landscape characteristics or processes of interest, whereas now the problem is one of how best to process and use the mass of high resolution data that it is possible to collect (Vericat *et al.*, 2016). In short, HRT data do not necessarily mean that research questions or hypotheses can be properly addressed (Lane and Chandler, 2003); rather, the point is that they have to be seen simply as part of the toolkit which helps us to better understand earth surface processes (Tarolli, 2014). An equally critical part of the toolkit is a framework or workflow that allows data to be collected and used correctly to address the research question(s) at hand. Key stages include the establishment of an appropriate Ground Control Point (GCP) network (Westoby *et al.*, 2012) and appropriate camera calibration (Micusík and Pajdla, 2006). Assessment of error, at various stages, is also important (Passalacqua *et al.*, 2015) and for this some

1
2 97 experimentation is often necessary. Thus, greater engagement with each stage of the
3
4 98 process is extremely important (Smith *et al.*, 2015).
5
6
7
8 99 The last decade has seen a significant rise of interest in the theory and practice of
9
10 100 river restoration (Smith *et al.*, 2014a). River restoration extends from localised actions
11
12 101 such as gravel augmentation to broader ecosystem restoration such as the connection
13
14 102 of river and floodplain areas through channel and flow re-naturalisation (Boon, 1998).
15
16
17 103 Lamouroux *et al.* (2015) highlight the need for science-based tools to reliably predict
18
19 104 the ecological responses to such restoration. These tools rely partly on the correct
20
21 105 characterisation of physical habitat conditions prior to the commencement of
22
23 106 restoration and the tracking of habitat changes that occur over time in response to the
24
25 107 restoration. However, such characterisation, which is now possible through the
26
27 108 acquisition of HRT data, has been argued to be missing in many restoration monitoring
28
29 109 projects (Olden *et al.*, 2014; Lamouroux *et al.*, 2015). The emergence of UAVs and
30
31 110 the application of SfM to UAV imagery can potentially help resolve this issue: i.e.
32
33 111 repeat topographic survey data allow assessment of the geomorphic ‘success’ of
34
35 112 restoration projects and, in turn, whether such physical habitat changes may lead to
36
37 113 improved Ecological Status (as defined in Europe by Water Framework Directive
38
39 114 criteria, European Union, 2000).
40
41
42
43
44
45
46 115 This paper addresses the question of how we can best use HRT data and SfM
47
48 116 techniques to assess geomorphic changes occurring in response to river restoration.
49
50 117 The paper presents a detailed workflow model of how HRT data can be obtained
51
52 118 effectively and how they can be used to aid assessment of geomorphic change. We
53
54 119 first provide some basic information on HRT acquisition and applications. Then we
55
56 120 present the workflow model designed to acquire and assess HRT information by
57
58 121 means of SfM photogrammetry applied to UAV-based imagery; it builds upon existing
59
60 122 generic workflows (e.g. Westoby *et al.*, 2012) to improve confidence in output from

consumer grade cameras and UAV platforms. As part of the presentation of this workflow we discuss the various issues that need to be considered at each stage, and cite key papers that provide greater details of specific methods or analyses. We then use a case study (Ben Gill, NW England) to show examples of analyses and outputs from each stage of the workflow. Finally, we summarise and discuss the insights provided by HRT data and SfM photogrammetry in the river restoration case study, and outline the broader relevance of the workflow model.

Digital Photogrammetry: workflow and its application to river restoration

Study area and context

The River Ehen (NW England, Figure 1) supports an internationally important population of the endangered mussel *Margaritifera margaritifera* (L.). As part of a programme of measures to improve habitat conditions in the Ehen for mussels, restoration work on one of its tributaries (Ben Gill) commenced in 2014. Ben Gill is a small (0.54 km²), high gradient (slope 25%) first order stream. Although it is not gauged, previous estimates suggest that it flows for approximately 23% of the time (Quinlan *et al.*, 2014a). In the 1970s Ben Gill was disconnected from the Ehen and diverted to Ennerdale Lake (see Figure 1B) to help increase lake storage and meet abstraction requirements in the region. The disconnection diverted the lower section of Ben Gill, such that rather than following its original course to the Ehen, water fell through a grill and was conveyed via an underground culvert to the lake. The original channel in the lower section has progressively terrestrialised in the 40 years since the diversion, becoming largely indistinguishable from the surrounding rough pasture land. Sediments delivered from the upper section, which accumulated around the grill, have been removed periodically and used locally as building material. However, concerns

1
2 148 over how this diversion might be limiting sediment supply to and flows in the Ehen
3
4 149 (and hence impacting the suitability of conditions for mussels) prompted plans to
5
6 150 reconnect it.
7
8
9
10 151 During the summer of 2014, a new channel was engineered for the lower section of
11
12 152 Ben Gill, following its original (pre-diversion) course. The channel was designed to
13
14 153 convey a 1 in 100 year flood, plus a 20% increment to accommodate potential
15
16 154 increases in discharge related to climate change. It was constructed 5 m wide and 0.5
17
18 155 m deep (mean values), with a generally semi-circular cross sectional shape (Figure
19
20 156 1C) (United Utilities, 2012). This new lower section of channel is approximately 300 m
21
22 157 long and has an average gradient of 9.4%. Once dug, the channel was lined with
23
24 158 cobble-size material (sizes between 20 and 250 mm *b* axis), with larger boulders along
25
26 159 the sides (up to 750 mm *b* axis). The new channel was reconnected on October 3rd,
27
28 160 2014, at which point water and sediments from Ben Gill were again able to enter the
29
30 161 main River Ehen (Figure 1B). Our objective was to monitor geomorphic changes in
31
32 162 Ben Gill, in order to quantify how much sediment would be delivered to the Ehen as a
33
34 163 result of the reconnection and the evolution of the engineered channel. Figure 2 shows
35
36 164 the timeline of the study while Figure 3 presents the workflow model designed to
37
38 165 provide a framework to assess geomorphic changes in Ben Gill.
39
40
41
42
43
44
45

46 166 ***Data acquisition***
47
48

49 167 The spatial coverage and resolution of image capture in photogrammetric studies
50
51 168 should be chosen to match research objectives. In fluvial applications, the areas
52
53 169 covered are frequently in the order of km², with variable flying altitudes (e.g. Javernick
54
55 170 *et al.*, 2014 [600m]; Tamminga *et al.*, 2014 [100m]; Dietrich, 2016 [200m]). While the
56
57 171 resolution achieved in such large spatial area studies can be remarkable, a much
58
59 172 higher resolution can be expected when the same technology is applied to a much
60
173 smaller area with a low flying altitude (e.g. in the case of Ben Gill, covering 300 m

channel length at <20 m altitude). Low altitude flights also have the advantage that, in the UK, they are below those needed for Civil Aviation Authority permissions (121.92 m, Civil Aviation Authority, 2015).

The fact that Ben Gill is an intermittent stream means that for most of the time the channel bed is exposed, enabling the collection of HRT data for its whole area. This avoids errors related to water surface reflection in submerged areas (as discussed by Tamminga *et al.*, 2014; Woodget *et al.*, 2014). Aerial images for the channel were collected using an 11 megapixel GoPro Hero 3+ Black Edition (Woodman Labs, Inc., USA). GoPro cameras are used increasingly for photogrammetry but the use of fisheye lenses (as present in the GoPro) has been criticised (e.g. James and Robson, 2012). We therefore undertook a series of camera tests prior to data collection (Figure 3); these tests were also designed to determine appropriate Ground Control Point (GCP) markers. First we evaluated different shapes, sizes and colours of GCP markers, to assess visibility and ease of picking out their centre points at multiple distances (i.e. at potential flight altitudes). Second, camera calibration parameters were obtained using AgiSoft Lens (AgiSoft LLC, 2015a; AgiSoft LLC, Russia). These parameters included the k_3 and k_4 distortion coefficients, which are advised when using fish-eye lenses for SfM (PhotoModeler, 2013). Third, once calibrated, an experiment was designed to test for the ability of the camera to capture details at different distances and to evaluate the errors associated with different flight altitudes. This experiment was conducted outdoors. Two A0 sized posters with attached coloured semi-spheres (of known sizes, from 1 to 10 cm diameter) were each glued to a board. Pictures were taken at multiple distances from the boards (5 m, then from 10 to 50 m at 10 m increments) to represent different flight altitudes. A local survey control network was set up by means of 4 targets installed around the field where the experiment was conducted, and markers placed on each corner of each board. A Leica

TCRP1201 Total Station (Leica Geosystems Inc.) was set up using the local control network and used to survey the position and shape of each of the painted semi-spheres. Additionally, 100 random points were surveyed on the flat surface of each of the boards. The point clouds obtained from the GoPro photographs taken at different distances from the boards were compared with the points surveyed by the Total Station. The results indicated that Root Mean Square Errors (RMSE) of the residuals of the elevations ranged from 0.015 to 0.192 m. Residuals were lowest at 5 m from the boards (RMSE= 0.015), and were consistent at 10 and 20 m (RMSE of 0.040 and 0.030 m respectively). At distances greater than 30 m from the boards, residuals were of the same magnitude as the size of the semi-spheres. Thus, the optimal flight altitude for this camera, given the RMSE values, was determined to be around 20 m. This altitude guarantees a sufficiently large image footprint and, given the camera's lens, minimal error for characterising channel properties (e.g. roughness).

Once flight altitude and camera tests were completed, 196 A3-sized white GCPs, marked with a black cross in the centre, were installed around the channel. GCPs are necessary to register all data to the same coordinate system. They are also the most common way to infer positional uncertainty in SfM (Passalacqua *et al.*, 2015) and, when distributed appropriately, can help with correction of the so-called 'dome effect' (which results from the use of exclusively vertical imagery; Smith and Vericat, 2015). Of the 196 GCPs, 178 were spread regularly in four parallel lines (two along each side of the channel), while the remaining 18 were scattered randomly at meanders to better capture channel planform where it was more complex. The same GCPs were used for all flights (i.e. we had a fixed control network) and were re-surveyed frequently to make sure none had moved. The total area studied covers approximately 0.06 km², with the GCPs therefore giving an average density of 3300 per km² (i.e. 33 GCPs per hectare). This is a very high density compared to other studies (e.g. Woodget *et al.*, 2014; 5.7

to 7.6 per hectare). All GCPs were surveyed using a Leica Viva GNSS (Leica Geosystems Inc.) differential rtk-GPS. The quality of the coordinates (3D quality) oscillated between 0.009 and 0.024 m.

Periodic UAV surveys were undertaken following the reconnection of the Ben Gill channel (Figure 2), timed to capture changes following high flow events. The camera was mounted on a DJI Phantom I UAV. Images were captured vertically, using a Zenmuse H3 2D gimbal camera mount. The time-lapse function of the camera allowed for image capture at 1 second intervals, with around 1100 images acquired per survey. The UAV was controlled manually on each survey. Test flights indicated that flying at 20 m altitude along 3 lines (both banks, then along the channel centreline) yielded necessary image overlap. As the channel was open and accessible along its full length, altitude and flight lines were controlled easily by walking alongside the UAV. Here we present data and outputs from 3 surveys to illustrate application of the workflow.

Data processing

Digital Photogrammetry: set up and application

Aerial images were post-processed using AgiSoft PhotoScan Professional (AgiSoft LLC, 2015b); the main steps are schematically represented in Figure 3. The number of images selected for each model was limited to a maximum of 500, in order to provide good overlap without over-extending the computing time required for processing. A first set of images was discarded using the 'Estimated Image Quality' from PhotoScan, which uses sharpness values to define quality (0 = blurred, 1 = very sharp). The standard approach is to discard images with sharpness values less than 0.5. However, we adopted a value of 0.85 which meant that only the very sharpest images were retained. Additional images were then discarded on the basis of 4 criteria: (i) over-

251 exposure to light, (ii) graininess due to high ISO values, (iii) objects (e.g. legs of the
252 UAV) hiding features of interest, and (iv) very high overlap between images (e.g. when
253 the UAV was static). The final selected images were then aligned in AgiSoft using the
254 calibration parameters acquired during the 'preparation and experimentation' phase.
255 The centre points of the GCPs were identified and adjusted manually on the images
256 for more accurate positioning. The coordinates of the GCPs were used to
257 georeference the sparse point cloud. The MVS algorithm implemented in the software
258 allowed creation of the final dense point cloud. AgiSoft provides the errors (in three
259 dimensions) of the GCPs used for the registration. These registration errors provide a
260 first indication of the quality of the point cloud, although strictly speaking they only
261 represent the error associated with the transformation (rotation, translation and
262 scaling) of the point clouds. We therefore used some of the GCPs as Check Point
263 (ChP) markers to assess the accuracy of the point cloud.

265 *Processing point clouds*

266 The steps reported above allowed the creation of very high-density point clouds (>20
267 million observations) which represented large and computationally demanding files.
268 To reduce the processing constraints, the raw point clouds were decimated using the
269 Topography Point Cloud Analysis Toolkit (ToPCAT) (Brasington *et al.*, 2012). ToPCAT
270 is now available within the Geomorphic Change Detection ArcMap extension (see
271 <http://gcd6help.joewheaton.org/>) and has been used by several authors (e.g.
272 Brasington *et al.*, 2012; Storz-Peretz and Laronne, 2013; Williams *et al.*, 2014; Smith
273 and Vericat, 2015). The point cloud decimation procedure followed the approach set
274 out by these authors, and allows the creation of gridded topographic information,
275 including statistical parameters for each cell.

Point cloud decimation was executed at two different resolutions. A 0.05 m resolution model was created and used to obtain the DEMs, which were then used to assess geomorphic changes. This resolution was chosen to be in agreement with the errors of the surveys (see 'Error analysis' section below). The minimum elevation within each cell was the statistical parameter used as ground elevation. These values were gridded using the *Topo to Raster* tool in ArcMap 10.3 (Esri® Inc., USA). The choice of interpolation method is important when the density and distribution of data points are poor (Chaplot *et al.*, 2006; Weng, 2006). In our case a formal interpolation was not required as the average point density per cell was high (up to 35). To complement the 0.05 m resolution model, a 0.25 m decimation was undertaken and used to generate sub-grid statistics that were used to characterise channel roughness. Among the statistics produced were the standard deviations of the detrended elevations within each cell. This statistic is being used increasingly as a metric of roughness across the Earth Sciences (Smith 2014); it is particularly useful as it represents how variable the micro-topography is in each cell, as a function of particle size variability and bedforms. For Ben Gill, the 0.25 m model was used to develop roughness maps. Roughness values are influenced by the size of the grid cells: if the grid is too small, all observations within a cell may fall on the same particle, while if the grid is too large, the deviation of the elevations will not be just determined by the size of the particles, but will be influenced by bedforms or by abrupt topographic changes (e.g. at banks). Thus, the selection of the grid cell size in this type of analysis is fundamental. For Ben Gill, grid cell size was determined based on the sediments used to line the new channel (maximum 250 mm *b* axis).

Analysing geomorphic change

1
2 301 Although direct comparison of point clouds is possible (Lague *et al.*, 2013), the most
3
4 302 commonly used approach to monitor geomorphic change is to compare two
5
6 303 successive DEMs through the production of DEMs of Difference (DoDs). DoDs have
7
8 304 been applied widely in fluvial geomorphology to estimate bed material transport rates
9
10 305 (Ashmore and Church, 1998; Church, 2006; Vericat *et al.*, 2016), as well as to analyse
11
12 306 channel changes (Brasington *et al.*, 2003; Lane *et al.*, 2003; Wheaton *et al.*, 2013) and
13
14 307 to help parameterise hydraulic models (e.g. Williams *et al.*, 2013). For Ben Gill, DoDs
15
16 308 were used to assess the magnitude and spatial patterns of geomorphic change as well
17
18 309 as to establish sediment budgets (e.g. Brasington *et al.*, 2003; Lane *et al.*, 2003;
19
20 310 Wheaton *et al.*, 2010b). In this paper we present DoDs produced from 3 flights, which
21
22 311 we use to assess changes occurring over two periods within the first 6 months of the
23
24 312 reconnection. The quality of the DEMs determines the level of confidence that can be
25
26 313 placed on assessment of change, and is discussed in the 'Error analysis' section.
27
28
29
30
31
32
33
34
35
36
37
38
39
40
41
42
43
44
45
46
47
48
49
50
51
52
53
54
55
56
57
58
59
60

315 *Obtaining orthophotos*

316 High resolution orthophotos (0.025 m cell) of the survey area were exported from
317 AgiSoft PhotoScan. Although these can be used for a variety of purposes (e.g. Vericat
318 *et al.*, 2009; Tamminga *et al.*, 2014), we used them to classify and quantify substrate
319 cover in Ben Gill, distinguishing between features of interest (substrate) and non-
320 interest (vegetation, fences, a footbridge etc.). Sediments in these orthophotos
321 (referred to henceforth as facies maps) were classified as coarse (gravel to boulder
322 sized material) or very fine material (sand and clay material). The 'Image
323 Classification' tool (ArcMap 10.3) was used to run a Maximum Likelihood Classification
324 of the orthophotos. Classified images were used to help interpret assessments of
325 change. Note that direct field-based validation of the classification was not undertaken.

326

Error analysis

Based on some of the general principles reported by Wheaton *et al.* (2010), the next key step in the workflow was to assess uncertainties in the DoDs. Uncertainty in the comparison of topographic models has been analysed critically by Brasington *et al.* (2000) and Lane *et al.* (2003). More recently, Wheaton *et al.* (2010) questioned the possibility of distinguishing real geomorphic change from noise when two DEMs are compared through DoDs. They developed different methods to account for uncertainty in DoDs, from simple to more complex ones. AgiSoft PhotoScan provides information on the error associated with the registration process. Additionally, it is possible to produce an estimation of the quality of the point cloud by using some of the GCPs as ChPs. For Ben Gill, differences between the real coordinates of the ChPs and their estimated coordinates (provided automatically by the software) was used as an indication of the 'measurement quality'. One third ($n = 64$) of the GCPs were used as ChPs, while the remainder ($n = 129$) were used as markers (i.e. for the registration of the point cloud). A bootstrapping resampling technique was implemented within AgiSoft to randomly select ChPs and calculate the errors (residuals) for all GCPs. After 1000 resamplings, (i) the standard deviation of these residuals was defined as the measurement uncertainty (or precision), while (ii) the mean of the residuals was considered as the accuracy.

Once the measurement of uncertainty of each model is assessed, a minimum Level of Detection threshold (minLoD) can be calculated. This minLoD allows what is considered as real topographic change to be distinguished from inherent noise (Fuller *et al.*, 2003). There are different methods to propagate the errors and identify the minLoD, ranging from a simple uniform distribution of the estimated DEM error to more complex statistical calculations of spatially distributed errors (see Brasington *et al.*,

2000; Lane *et al.*, 2003; Wheaton *et al.*, 2010b; Milan *et al.*, 2011). The conventional uniform approach can be sufficient for low topographic complexity environments, but tends to be overly-conservative compared to the spatially distributed approach (Milan *et al.*, 2011). A more sophisticated statistical model of DEM surface error propagation (Brasington *et al.*, 2003; Lane *et al.*, 2003; Wheaton *et al.*, 2010b) that helps detect lower magnitude geomorphic changes (erosion and/or deposition) was used for Ben Gill. This involves calculation of the spatial distribution of *t*-scores (Lane *et al.* 2003) using:

$$t = \frac{Z_2 - Z_1}{\sqrt{(\varepsilon_{DEM_1})^2 + (\varepsilon_{DEM_2})^2}}$$

with Z_2 and Z_1 being the elevation in a given cell of the most recent and oldest DEM respectively, and ε_{DEM_2} and ε_{DEM_1} their respective error terms (in our case the standard deviation of the ChP residuals).

In this approach each cell is attributed a *t*-score. Change observed in each cell is estimated to be true or false, based on the chosen minimum threshold of *t*-score (e.g. 1.28 for 80% Confidence Interval [CI], 1.96 for 95% CI). Therefore, by rearranging the above equation (Brasington *et al.*, 2003), a minLoD can be calculated as:

$$minLoD = t \sqrt{(\varepsilon_{DEM_1})^2 + (\varepsilon_{DEM_2})^2}$$

Consequently, when the difference in elevation ($Z_2 - Z_1$) in a given cell is smaller than the minLoD, the change is considered uncertain at the chosen confidence interval (*t*). This does not mean that no change occurred in the cell, but simply that the estimated changes are subject to such uncertainty that it is unwise to use them.

Evaluating geomorphic responses to river restoration: the case of Ben Gill and the River Ehen

High resolution orthophotos

Table 1 shows the main parameters for each of the three flights, with an example orthophoto presented in Figure 4A. Data for this orthophoto were acquired in April 2015; the registration error during post-processing was 0.039 m. It was exported at 0.025 m resolution and used for classification of vegetation, gravel and fine sediment (Figure 4B).

Image classification can be of great use for critically reviewing geomorphic changes inferred from DoDs. For example, vegetation may be wrongly interpreted as geomorphic change due to seasonal patterns of growth and decay. Vegetation was not a major issue in Ben Gill because it was more or less absent from the active channel (Figure 4B). Areas determined as fine sediments were very flat and had low roughness values. Thus, geomorphic changes appearing in such areas are very likely to be real ones. Conversely, areas identified as being composed of coarser material had different values of roughness and, potentially, the uncertainty surrounding estimates of topographic change monitored in these areas will be greater.

Surface and roughness models

Table 1 presents the average point density of the three Ben Gill point clouds, while Table 2 shows the registration errors and the uncertainty and accuracy of each one. On average, point clouds had more than 1000 points/m². Values for registration errors and model uncertainty were very similar and never exceeded 0.06 m. These results indicate that the workflow allowed the collection of high density and accurate HRT data for the Ben Gill channel. Figure 4C shows an example of one of the DEMs.

398 An example of using the detrended standard deviation of elevations as an indicator of
399 bed roughness is shown in Figure 5. As is evident in the Figure, the banks of the
400 channel are formed by relatively rough (i.e. coarse) sediments while finer sediments
401 are present mostly in the bed of the channel. Roughness values for the flat parts of
402 the channel are in agreement with sediment sizes observed in the field. However, as
403 Figure 1C shows, the convex parts of the bends were covered with relatively fine
404 material, something which is not evident solely from the roughness values. The
405 overestimation of roughness in these convex areas may be attributed to the size of the
406 grid for which roughness was calculated (0.25 m) in relation to the sharpness of the
407 bank. A similar effect is observed with the presence of bedforms in river channel beds.
408 If the grid of the cell used to calculate the sub-grid statistics using ToPCAT is larger
409 than the bank line (or the bedform if the case), the detrending procedure does not only
410 provide the variability of the elevations mainly attributed to the particles, but also the
411 variation attributed to the bank slope (or to the bedform). A simple way to overcome
412 the problem is to clip these zones out from the analyses (using the orthophoto
413 classification data); alternatively, the grid resolution in these zones could be changed.
414 These solutions require some additional work, but their products are advantageous as
415 they allow the production of continuous maps of roughness which can be very valuable
416 for the assessment of habitat conditions, their evolution over time, and for the
417 parametrisation of hydraulic models, all of which are extremely useful in restoration
418 applications.

419 Three close-ups are presented as part of Figure 5 to illustrate different features in the
420 new channel. Figure 5A shows contrasting roughness around an erosional area in the
421 downstream section of the channel. While the main layer of clay is flat and constant,
422 abrupt lines of coarse sediment are observed. Figure 5B shows a rather uniform
423 section (except for the margins) in the middle section of the channel. Although the

roughness values here are generally similar, several facies can be observed; this is in agreement with visual observation of the orthophotos. Finally, in 5C a more complex and heterogeneous distribution of roughness is shown for an upstream section of the channel. The heterogeneity is related mainly to the large boulders which were placed here at the time of channel construction.

Roughness values obtained by this approach tend to correlate well with the median particle size of the sediments, as already indicated by Brasington *et al.* (2012). Although the correlation presented by these authors requires site-specific validation, it is evident that roughness maps can potentially be transformed into particle size maps that may add value to the information provided by image classification; in turn, this aids understanding of changes in bed texture in time and/or space.

Geomorphic change detection

Topographic changes (Figure 6) were thresholded by applying a statistical minLoD as described in the 'Error Analysis' section. In this case we used $t = 1.28$ (i.e. 80% CI). A value of $t = 1.96$ (i.e. 95% CI) was also applied to see how changing the confidence interval affected the results (Table 3). By taking a more or a less conservative t value, the number of cells considered as recording real changes in Ben Gill, as well as the estimate of net change, varied appreciably.

Figure 6 and Table 3 indicate that erosion was the dominant process in Ben Gill over the study period (at 80% CI, 79.5% of the topographic changes were characterised as erosion), with only a small part at the downstream end of the channel experiencing deposition. Two main erosional sections are evident. Of these, the downstream section underwent the most significant changes at both of the time intervals considered here, although the scale of change was greater between January and April 2015 (Figure 6B) than between October 2014 and January 2015 (Figure 6A). The first

1
2 449 DoD (Figure 6A) revealed little lateral change but extensive vertical erosion, with
3
4 450 maximum levels of erosion and deposition of 1.07 m and 0.50 m respectively. Figure
5
6 451 6B illustrates the more intense change that occurred between January and April 2015,
7
8
9 452 with erosion of more than 1 m in both lateral and vertical dimensions in some areas.
10
11 453 The channel was subject to vertical deepening and bank erosion, as well as significant
12
13 454 deposition at the lower end of the channel. Maximum levels of erosion (1.40 m) and
14
15 455 deposition (0.62 m) were higher than observed in the first period. The evolution of the
16
17
18 456 channel over the whole of the study period was also evident in changes in its long
19
20 457 profile (Figure 7). There was an upstream propagation of two knick-points, a
21
22 458 phenomenon influencing spatio-temporal changes in patterns of erosion along the
23
24 459 channel.
25
26
27
28

29 460 Erosion from Ben Gill has led to the development of a confluence bar where it
30
31 461 discharges into the Ehen (Figure 4A). This bar has grown progressively over the
32
33 462 survey period and, by April 2015, was 34 m long and 12 m wide.
34
35
36

37 463 ***Sediment budget***
38
39

40 464 Total volumes of erosion and deposition, together with the net volume change, are
41
42 465 given in Table 3. The estimate of net change in the second period (January to April
43
44 466 2015; -120m³) is four times higher than that for the first (October 2014 to January
45
46 467 2015; -30m³). Although the net volume of change is often used as a sediment budget
47
48 468 term, strictly speaking it is only part of the budget since input or output values of
49
50 469 sediment for the study reach are required to properly resolve the total budget.
51
52
53
54
55 470

58 471 **Discussion**
59
60

472 ***Application of the workflow to Ben Gill***

1
2 473 The workflow (Figure 3) was designed to capture the geomorphic evolution of the
3
4 474 newly created Ben Gill channel. It was based on that used by others (e.g. Westoby *et*
5
6 475 *al.*, 2012; Javernick *et al.*, 2014; Tamminga *et al.*, 2014), but modified to reflect two
7
8
9 476 important points. (i) As we were using a relatively low resolution camera fitted with a
10
11 477 fish-eye lens, it was important to add preliminary stages to the workflow related to
12
13 478 camera calibration, lens distortion and assessment of flight altitudes. (ii) As we were
14
15
16 479 interested in assessing change, rather than simply characterising topography at a
17
18 480 single point in time (as in Ely *et al.*, 2016), it was important to add a stage to the
19
20 481 workflow related to the assessment of model accuracy. The large number of markers,
21
22 482 some used as GCPs and other as ChPs within a bootstrapping procedure, was critical
23
24
25 483 to this assessment.
26
27

28
29 484 Changes in Ben Gill proved to be far greater than the minimum level of detection and
30
31 485 so could be quantified confidently using a photogrammetric approach. Our approach
32
33 486 was also practical and affordable. At current prices, the UAV (DJI Phantom I) costs
34
35 487 £275, the GoPro Hero 3+ £265 and the Gimbal camera mount is around £200 (total
36
37 488 cos t= £740), while the set up and removal of the GCP network took only around 3
38
39 489 hours and 3-4 passes of the channel (as required to capture the necessary images)
40
41 490 took approximately 25 minutes. Others have already stressed how UAV-based
42
43 491 photogrammetry is cost effective and, indeed, may become the standard for
44
45 492 topography production (Carbonneau and Dietrich, 2016). While SfM photogrammetry
46
47 493 is not, in itself, able to ensure that river restoration initiatives are successful, it can
48
49 494 prove critical for the proper assessment of whether or not projects are achieving their
50
51 495 geomorphic objectives.
52
53
54
55
56

57
58 496 The analysis of the data derived from SfM photogrammetry indicated that the newly
59
60 497 created channel has undergone net erosion in the first 6 months following its
498 connection to the Ehen. This has several implications in terms of meeting the

objectives of the wider River Ehen restoration project. First and most importantly, the objective of re-establishing more dynamic and hence natural fluvial processes in the downstream reach of the Ehen seems to be on the way to being met. Previous work (Quinlan *et al.*, 2014a) has shown that the study section had become extremely stable, with little movement of either coarse or fine material. Although we have monitored only the first few months following the reconnection, the DoDs and related sediment budgets illustrate the magnitude of sediment volume now being delivered to the Ehen. Increased dynamism is evident from the development of a bar at the Ehen-Ben Gill confluence. Ongoing analysis of this bar using multi-temporal DEMs, in parallel with studies of bed mobility (marked tracers), will allow us to assess quantitatively its temporal evolution in relation to competent discharges in the Ehen, and hence the timing of sediment delivery further down into the Ehen system and how this is changing the sedimentary conditions previously reported (Quinlan *et al.*, 2014a). The second important point to come from the photogrammetric analysis is that a large proportion of the newly engineered channel is composed of very fine material. This material is part of the alluvial fan which the channel cuts across (a fan formed by the original Ben Gill), but which has become exposed as a result of the erosion of the coarse material used to line the new channel. This is notable within the context of *M. margaritifera* habitat, as fine material potentially contributes to increases in suspended sediment in the Ehen at times when Ben Gill is flowing. Our workflow allows us to keep track of the erosion of this material and the hence risks posed to mussels by high suspended sediment concentrations. Although they can survive short-lived periods of high suspended sediment concentrations, the deposition of fines on the bed can create sub-optimum conditions for mussels, especially juveniles (Quinlan *et al.*, 2014b). Ongoing analysis of Ben Gill will provide a more in-depth understanding of the processes occurring in the channel, as well as the volumes and timing of material delivered to the Ehen.

From a technical point of view, the workflow provides a formalised framework within which various testing and calibration procedures can be undertaken. We have shown that, with careful calibration, use and testing, fish-eye lenses such as fitted to GoPro cameras can be used for photogrammetric applications in fluvial geomorphology. Although image quality is somewhat lower than from non-distorted lens (Thoeni *et al.*, 2014), an appropriate calibration of the camera combined with particular attention to the GCP network setup and a good understanding of the way the SfM software works can lead to scientifically robust and defensible results. These results stemmed from the fact that: (i) we used the highest resolution GoPro available (at the time of study), (ii) flying altitude was rather low (12 to 16 m), (iii) flying speed was low, in order to reduce shutter-speed induced blur, (iv) overlap between images was very high, (v) *a-priori* calibration of the camera included k_3 and k_4 distortion parameters, (vi) flight paths were controlled and images selected so that the channel (i.e. area of interest) was in the centre of the images, reducing edge-related distortions, and (vii) the dome effect was greatly reduced by the very high density of GCPs. Together these elements of the workflow proved key to the assessment of changes in Ben Gill. Although it is possible to use mini GPS systems fitted to drones to allow direct georeferencing of images, this is currently at the cost of accuracy (Carbonneau and Dietrich, 2016). Thus, the high density control network remains critical especially in cases where the detection of geomorphic change relies on high accuracy.

This workflow allowed to reach the maximum capacity of the equipment used for the study. Nonetheless, there are other technologies available that might improve upon what we have done. Heavy payload drones capable of carrying digital single-lens reflex cameras (with flat lenses and higher resolution), could, for example, improve the quality of the results and outputs. Similarly, the use of GPS flight assistance and

1
2 551 autopilot in newer generation drones would help optimise flying paths and altitudes in
3
4 552 order to improve image overlap and flight efficiency.
5
6
7
8 553 The high density control network ensured the high quality of the point cloud produced
9
10 554 from our camera and assessment of model accuracy and precision. This is important
11
12 555 for all river restoration studies, but is likely to be particularly critical in cases where the
13
14 556 magnitude of the response to intervention proves to be lower than observed in Ben
15
16
17 557 Gill.

18
19
20 558 In relation to the assessment and application of a minLoD in Ben Gill, deposition was
21
22 559 more affected by thresholding than erosion (Table 3). This is in general agreement
23
24 560 with other studies (e.g. Brasington *et al.*, 2003; Wheaton *et al.*, 2010b) which have
25
26 561 stressed the limits of interpreting DoDs and sediment budget estimates. Although
27
28 562 applying a lower CI results in lower information loss, it can be at the cost of a less
29
30 563 realistic or overly simplistic estimation of uncertainties. Wheaton *et al.* (2010) argue
31
32 564 that using a Fuzzy Inference System function could help improve spatially variable
33
34 565 estimates of surface representation uncertainties.
35
36
37
38
39
40 566

41
42
43 567 ***Wider relevance***

44
45
46 568 As highlighted by several authors (e.g. Micheletti *et al.*, 2014; Tarolli, 2014; Smith *et*
47
48 569 *al.*, 2015 and others), the application of SfM photogrammetry has become very
49
50 570 affordable. When applied with a solid testing procedure prior to data acquisition, it can
51
52 571 provide high quality and insightful data. The potential benefits of applying such
53
54 572 techniques to monitor and understand the post-restoration geomorphic evolution of
55
56 573 river channel habitat is rather self-evident: not only can photogrammetry provide
57
58 574 quantitative evidence of the geomorphic success or failure of a project, but it can also
59
60 575 help predict likely future changes, e.g. when combined with hydraulic modelling.

Williams *et al.* (2013), Tamminga *et al.* (2014) and Javernick *et al.* (2015), for instance, have successfully used DEMs derived from SfM photogrammetry to run 2D hydraulic models, while Smith *et al.* (2014b) provide comparisons of hydraulic models developed using SfM photogrammetry. Overall, SfM-based DEMs form a rich and detailed support for hydrological and hydraulic modelling.

Physical habitat complexity and heterogeneity are key influences on ecological diversity (Allan and Castillo, 2007), so being able to quantify these aspects of the habitat template of rivers properly is fundamental to understanding ecological responses to restoration measures. As SfM photogrammetry provides information that can be used to characterise habitat continuously at scales ranging from the grain to the reach, it can provide the basis for much improved representation of physical habitat. Thus, we suggest that it should be used more widely in river restoration monitoring programmes to gather information that is important both geomorphologically and ecologically.

Submerged areas constrain the application of photogrammetry due to the adverse effects of turbidity, turbulence, light penetration depth, and light refraction at the air-water interface (Lane, 2000; Westaway *et al.*, 2000; Woodget *et al.*, 2014). However, there are increasing numbers of examples to show that channel bathymetry can successfully be extracted from aerial images (e.g. Westaway *et al.*, 2001; Lane *et al.*, 2010; Tamminga *et al.*, 2014; Woodget *et al.*, 2014; Javernick *et al.*, 2015). In cases where the nature of the river may preclude the application of photogrammetry altogether (e.g. presence of dense riparian vegetation) alternative tools exist to collect high quality topographic information (e.g. Acoustic Doppler Current Profilers, Williams *et al.*, 2013). Thus, while the tools used to produce HRT data may differ from one project to another, the workflow detailed in Figure 3 remains applicable to all, as it simply provides the framework for consistent and robust analyses.

1
2
3
4
5
6
7
8
9
10
11
12
13
14
15
16
17
18
19
20
21
22
23
24
25
26
27
28
29
30
31
32
33
34
35
36
37
38
39
40
41
42
43
44
45
46
47
48
49
50
51
52
53
54
55
56
57
58
59
60

Concluding remarks

We have shown that SfM photogrammetry based on images collected using a UAV-mounted GoPro camera can be used to assess the effectiveness of river restoration measures. However, it is important to follow a procedure that is tailored to individual projects and the equipment used. The workflow presented here was successfully applied to the River Ehen restoration project, allowing us to obtain high resolution topographic data as well as orthophotos from which multiple outputs were extracted (DEMs, DoDs, roughness and facies maps). Thus, the workflow fulfilled its main purpose of providing key information on the geomorphic evolution of the channel, notably the amount of material transported and potentially available in the sediment-starved system downstream. When applied with appropriate preparation and experimentation prior to field data collection, the SfM photogrammetry can greatly improve the characterisation of channel morphology that should be a fundamental part of all river restoration projects.

It is likely that the current project is a rare example of restoring natural fluvial dynamics in a sediment-starved system using non-invasive techniques. The re-introduction of sediment to the Ehen has been achieved not by artificial augmentation, but by reinstating a functional high energy headwater tributary and its catchment. While Ben Gill itself is not critical ecologically, its hydrologic and geomorphic functioning is fundamental to the restoration of the Ehen system. Ongoing monitoring of the evolution of Ben Gill, together with a thorough assessment of its effects on the Ehen geomorphology and the ecological responses to these changes, will eventually allow us to fully assess the success of the Ehen restoration project.

Acknowledgements

This research is funded by the Environment Agency and United Utilities whose support is gratefully acknowledged. Some of the methods employed in this work have been tested on the background of the results obtained in MorphSed (www.morphsed.es), a research project funded by the Spanish Ministry of Economy and Competiveness and the European Regional Development Fund Scheme (FEDER; CGL2012-36394). The second author is funded by a Ramon y Cajal Fellowship (RYC-2010-06264). Authors acknowledge the support from the Economy and Knowledge Department of the Catalan Government through the Consolidated Research Group 'Fluvial Dynamics Research Group' (2014 SGR 645). The authors thank Manel Llena from the University of Lleida for his help and contribution to the camera calibration experiments. We are also grateful to the three anonymous reviewers and the editors for their comments that greatly improved the manuscript.

List of abbreviations

ChP: Check Point

CI: Confidence Interval

DEM: Digital Elevation Model

DoD: DEM of Difference

GCD: Geomorphic Change Detection

GCP: Ground Control Point

GIS: Geographic Information System

HRT: High Resolution Topography

LiDAR: airborne laser surveying technology, created from "Light" and "raDAR"

minLoD: minimum Level of Detection

1
2
3
4
5
6
7
8
9
10
11
12
13
14
15
16
17
18
19
20
21
22
23
24
25
26
27
28
29
30
31
32
33
34
35
36
37
38
39
40
41
42
43
44
45
46
47
48
49
50
51
52
53
54
55
56
57
58
59
60

- 652 MVS: Multi-View Stereo
- 653 rtk-GPS: real-time kinematic Global Positioning System
- 654 SfM: Structure-from-Motion
- 655 ToPCAT: Topographic Point Cloud Analysis Toolkit
- 656 UAV: Unmanned Aerial Vehicle
- 657 **Conflicts of interest**
- 658 The authors declare no conflict of interest.

Reference list

- AgiSoft LLC. 2015a. AgiSoft Lens. Version 0.4.2 beta [online] Available from:
<http://www.agisoft.ru/products/lens>.
- AgiSoft LLC. 2015b. Agisoft PhotoScan Professional Edition. Version 1.2.3 [online]
Available from: <http://www.agisoft.com/downloads/installer/>.
- Allan JD, Castillo MM. 2007. Stream Ecology: Structure and Function of Running
Waters. 2nd Ed. Springer: Dordrecht, The Netherlands.
- Ashmore PE, Church M. 1998. Sediment transport and river morphology: a paradigm
for study. In *Gravel-Bed Rivers in the Environment*, Klingeman PC, Beschta RL,
Komar PD, and Bradley JB (eds). Water Resource Publ.: Highland Ranch, CO; 115–
148.
- Bangen SG, Wheaton JM, Bouwes N, Bouwes B, Jordan C. 2014. A methodological
intercomparison of topographic survey techniques for characterizing wadeable
streams and rivers. *Geomorphology* **206**: 343–361. DOI:
[10.1016/j.geomorph.2013.10.010](https://doi.org/10.1016/j.geomorph.2013.10.010).
- Boon PJ. 1998. River restoration in five dimensions. *Aquatic Conservation: Marine
and Freshwater Ecosystems* **8**: 257–264.
- Brasington J, Langham J, Rumsby B. 2003. Methodological sensitivity of
morphometric estimates of coarse fluvial sediment transport. *Geomorphology* **53**:
299–316. DOI: [10.1016/S0169-555X\(02\)00320-3](https://doi.org/10.1016/S0169-555X(02)00320-3).
- Brasington J, Rumsby BT, McVey RA. 2000. Monitoring and modelling
morphological change in a braided gravel-bed river using high resolution GPS-based
survey. *Earth Surface Processes and Landforms* **25**(9): 973–990. DOI:
[10.1002/1096-9837](https://doi.org/10.1002/1096-9837).
- Brasington J, Vericat D, Rychkov I. 2012. Modeling river bed morphology,

- roughness, and surface sedimentology using high resolution terrestrial laser scanning. *Water Resources Research* **48**(11): 1–18. DOI: 10.1029/2012WR012223.
- Carbonneau PE, Dietrich JT. 2016. Cost-Effective Non-Metric Photogrammetry from Consumer-Grade sUAS: Implications for Direct Georeferencing of Structure from Motion Photogrammetry. *Earth Surface Processes and Landforms* DOI: 10.1002/esp.4012. [online] Available from: <http://doi.wiley.com/10.1002/esp.4012>.
- Chaplot V, Darboux F, Bourennane H, Leguédois S, Silvera N, Phachomphon K. 2006. Accuracy of interpolation techniques for the derivation of digital elevation models in relation to landform types and data density. *Geomorphology* **77**(1–2): 126–141. DOI: 10.1016/j.geomorph.2005.12.010.
- Church M. 2006. Bed Material Transport and the Morphology of Alluvial River Channels. *Annual Review of Earth and Planetary Sciences* **34**(1): 325–354. DOI: 10.1146/annurev.earth.33.092203.122721.
- Civil Aviation Authority. 2015. Unmanned Aircraft System Operations in UK Airspace - Guidance [online] Available from: <http://www.caa.co.uk/application.aspx?catid=33&pagetype=65&appid=11&mode=detail&id=415>.
- Dietrich JT. 2016. Riverscape mapping with helicopter-based Structure-from-Motion photogrammetry. *Geomorphology* **252**: 144–157. DOI: 10.1016/j.geomorph.2015.05.008.
- Ely JC, Graham C, Barr ID, Rea BR, Spagnolo M, Evans J. 2016. Using UAV acquired photography and structure from motion techniques for studying glacier landforms: application to the glacial flutes at Isfallsglaciären. *Earth Surface Processes and Landforms* DOI: 10.1002/esp.4044. [online] Available from: <http://doi.wiley.com/10.1002/esp.4044>.

- European Union. 2000. Directive 2000/60/EC of the European Parliament and of the Council of 23 October 2000 establishing a framework for Community action in the field of water policy. *Official Journal of the European Communities* **L237**: 1–73.
- Fuller IC, Large ARG, Charlton ME, Heritage GL, Milan DJ. 2003. Reach-scale sediment transfers: an evaluation of two morphological budgeting approaches. *Earth Surface Processes and Landforms* **28**(8): 889–903. DOI: 10.1002/esp.1011.
- Heritage GL, Milan DJ. 2009. Terrestrial Laser Scanning of grain roughness in a gravel-bed river. *Geomorphology* **113**(1–2): 4–11. DOI: 10.1016/j.geomorph.2009.03.021.
- James MR, Robson S. 2012. Straightforward reconstruction of 3D surfaces and topography with a camera: Accuracy and geoscience application. *Journal of Geophysical Research: Earth Surface* **117**(3) DOI: 10.1029/2011JF002289.
- Javernick L, Brasington J, Caruso B. 2014. Modeling the topography of shallow braided rivers using Structure-from-Motion photogrammetry. *Geomorphology* **213**: 166–182. DOI: 10.1016/j.geomorph.2014.01.006.
- Javernick L, Hicks DM, Measures R, Caruso B, Brasington J. 2015. Numerical modelling of braided rivers with Structure-from-Motion-derived terrain models. *River Research and Applications* **32**(5): 1071–1081. DOI: 10.1002/rra.
- Lague D, Brodu N, Leroux J. 2013. Accurate 3D comparison of complex topography with terrestrial laser scanner: Application to the Rangitikei canyon (N-Z). *ISPRS Journal of Photogrammetry and Remote Sensing* **82**: 10–26. DOI: 10.1016/j.isprsjprs.2013.04.009.
- Lamouroux N, Gore JA, Lepori F, Statzner B. 2015. The ecological restoration of large rivers needs science-based, predictive tools meeting public expectations: An overview of the Rhône project. *Freshwater Biology* **60**(6): 1069–1084. DOI:

- 734 10.1111/fwb.12553.
- 735 Lane SN. 2000. The measurement of river channel morphology using digital
736 photogrammetry. *Photogrammetric Record* **16**(96): 937–961. DOI: 10.1111/0031-
737 868X.00159.
- 738 Lane SN, Chandler JH. 2003. The generation of high quality topographic data for
739 hydrology and geomorphology: new data sources, new applications and new
740 problems. *Earth Surface Processes and Landforms* **28**: 229–230. DOI:
741 10.1002/esp.479.
- 742 Lane SN, Westaway RM, Hicks DM. 2003. Estimation of erosion and deposition
743 volumes in a large, gravel-bed, braided river using synoptic remote sensing. *Earth
744 Surface Processes and Landforms* **28**(3): 249–271. DOI: 10.1002/esp.483.
- 745 Lane SN, Widdison PE, Thomas RE, Ashworth PJ, Best JL, Lunt IA, Sambrook
746 Smith GH, Simpson CJ. 2010. Quantification of braided river channel change using
747 archival digital image analysis. *Earth Surface Processes and Landforms* **35**(8): 971–
748 985. DOI: 10.1002/esp.2015.
- 749 Micheletti N, Chandler JH, Lane SN. 2014. Investigating the geomorphological
750 potential of freely available and accessible structure-from-motion photogrammetry
751 using a smartphone. *Earth Surface Processes and Landforms* **40**(4): 473–486. DOI:
752 10.1002/esp.3648.
- 753 Micheletti N, Chandler JH, Lane SN. 2015. Structure from Motion (SfM)
754 Photogrammetry. In *Geomorphological Techniques*, Cook SJ, Clarke JH, and N. LS
755 (eds). British Society for Geomorphology: London, UK; 1–12.
- 756 Micusík B, Pajdla T. 2006. Structure from motion with wide circular field of view
757 cameras. *IEEE transactions on pattern analysis and machine intelligence* **28**(7):
758 1135–1149. DOI: 10.1109/TPAMI.2006.151.

- 759 Milan DJ, Heritage GL, Large ARG, Fuller IC. 2011. Filtering spatial error from
760 DEMs: Implications for morphological change estimation. *Geomorphology* **125**(1):
761 160–171. DOI: 10.1016/j.geomorph.2010.09.012.
- 762 Olden JD, Konrad CP, Melis TS, Kennard MJ, Freeman MC, Mims MC, Bray EN,
763 Gido KB, Hemphill NP, Lytle D a., McMullen LE, Pyron M, Robinson CT, Schmidt JC,
764 Williams JG. 2014. Are large-scale flow experiments informing the science and
765 management of freshwater ecosystems? *Frontiers in Ecology and the Environment*
766 **12**(3): 176–185. DOI: 10.1890/130076.
- 767 Passalacqua P, Belmont P, Staley DM, Simley JD, Arrowsmith JR, Bode CA, Crosby
768 C, DeLong SB, Glenn NF, Kelly SA, Lague D, Sangireddy H, Schaffrath K, Tarboton
769 DG, Wasklewicz T, Wheaton JM. 2015. Analyzing high resolution topography for
770 advancing the understanding of mass and energy transfer through landscapes: A
771 review. *Earth-Science Reviews* **148**: 174–193. DOI:
772 10.1016/j.earscirev.2015.05.012.
- 773 PhotoModeler. 2013. Using the GoPro Hero 3 for 3D Photogrammetry Modeling and
774 Measuring [online] Available from: [http://info.photomodeler.com/blog/using-the-](http://info.photomodeler.com/blog/using-the-gopro-hero-3-for-3d-photogrammetry-modeling-and-measuring/)
775 [gopro-hero-3-for-3d-photogrammetry-modeling-and-measuring/](http://info.photomodeler.com/blog/using-the-gopro-hero-3-for-3d-photogrammetry-modeling-and-measuring/). (Accessed 8 August
776 2014).
- 777 Quinlan E, Gibbins CN, Batalla RJ, Vericat D. 2014a. Impacts of Small Scale Flow
778 Regulation on Sediment Dynamics in an Ecologically Important Upland River.
779 *Environmental Management* **55**: 671–686. DOI: 10.1007/s00267-014-0423-7.
- 780 Quinlan E, Gibbins CN, Malcolm I, Batalla RJ, Vericat D, Hastie L. 2014b. A review
781 of the physical habitat requirements and research priorities needed to underpin
782 conservation of the endangered freshwater pearl mussel *Margaritifera margaritifera*.
783 *Aquatic Conservation: Marine and Freshwater Ecosystems* **124**: 107–124. DOI:
784 10.1002/aqc.2484.

- 785 Smith B, Clifford NJ, Mant J. 2014a. The changing nature of river restoration. *WIREs*
786 *Water* **1**(3): 249–261. DOI: 10.1002/wat2.1021.
- 787 Smith MW, Carrivick JL, Hooke J, Kirkby MJ. 2014b. Reconstructing flash flood
788 magnitudes using “Structure-from-Motion”: A rapid assessment tool. *Journal of*
789 *Hydrology* **519**: 1914–1927. DOI: 10.1016/j.jhydrol.2014.09.078.
- 790 Smith MW, Carrivick JL, Quincey DJ. 2015. Structure from motion photogrammetry
791 in physical geography. *Progress in Physical Geography* **40**(2): 247–275. DOI:
792 10.1177/0309133315615805.
- 793 Smith MW, Vericat D. 2015. From experimental plots to experimental landscapes:
794 Topography, erosion and deposition in sub-humid badlands from Structure-from-
795 Motion photogrammetry. *Earth Surface Processes and Landforms* **40**(12): 1656–
796 1671. DOI: 10.1002/esp.3747.
- 797 Storz-Peretz Y, Laronne JB. 2013. Morphotextural characterization of dryland
798 braided channels. *Bulletin of the Geological Society of America* **125**(9–10): 1599–
799 1617. DOI: 10.1130/B30773.1.
- 800 Tamminga A, Hugenholtz C, Eaton B, Lapointe M. 2014. Hyperspatial remote
801 sensing of channel reach morphology and hydraulic fish habitat using an Unmanned
802 Aerial Vehicle (UAV): a first assessment in the context of river research and
803 management. *River Research and Applications* **31**(3): 379–391. DOI:
804 10.1002/rra.2743.
- 805 Tarolli P. 2014. High-resolution topography for understanding Earth surface
806 processes: Opportunities and challenges. *Geomorphology* **216**: 295–312. DOI:
807 10.1016/j.geomorph.2014.03.008.
- 808 Thoeni K, Giacomini A, Murtagh R, Kniest E. 2014. A comparison of multi-view 3D
809 reconstruction of a rock wall using several cameras and a laser scanner.

- 810 *Proceedings of ISPRS Technical Commission V Symposium XL(5)*: 573–580. DOI:
- 811 10.5194/isprsarchives-XL-5-573-2014.
- 812 United Utilities. 2012. Hydrodynamic and Sediment Transport Modelling Report -
- 813 Project Name : Ennerdale and Ben Gill Project No : 80020012.
- 814 Vericat D, Brasington J, Wheaton J, Cowie M. 2009. Accuracy assessment of aerial
- 815 photographs acquired using lighter-than-air blimps: low-cost tools for mapping river
- 816 corridors. *River Research and Applications* **25**: 985–1000. DOI: 10.1002/rra.
- 817 Vericat D, Wheaton JM, Brasington J. 2016. Revisiting the morphological approach:
- 818 opportunities and challenges with repeat high resolution topography. *Gravel-bed*
- 819 *Rivers Series* (accepted).
- 820 Weng Q. 2006. An Evaluation of Spatial Interpolation Accuracy of Elevation Data. In
- 821 *Progress in Spatial Data Handling*, Rield A, Kainz W, and Elmes GA (eds). Springer-
- 822 Verlag: Berlin; 805–824.
- 823 Westaway RM, Lane SN, Hicks DM. 2000. The development of an automated
- 824 correction procedure for digital photogrammetry for the study of wide, shallow,
- 825 gravel-bed rivers. *Earth Surface Processes and Landforms* **25**: 209–226. DOI:
- 826 10.1002/(SICI)1096-9837.
- 827 Westaway RM, Lane SN, Hicks MD. 2001. Remote Sensing of Clear-Water, Shallow,
- 828 Gravel-Bed Rivers Using Digital Photogrammetry. *Photogrammetric Engineering &*
- 829 *Remote Sensing* **67**(11): 1271–1281.
- 830 Westoby MJ, Brasington J, Glasser NF, Hambrey MJ, Reynolds JM. 2012.
- 831 “Structure-from-Motion” photogrammetry: A low-cost, effective tool for geoscience
- 832 applications. *Geomorphology* **179**: 300–314. DOI: 10.1016/j.geomorph.2012.08.021.
- 833 Wheaton JM, Brasington J, Darby SE, Kasprak A, Sear D, Vericat D. 2013.
- 834 Morphodynamic signatures of braiding mechanisms as expressed through change in

1
2 835 sediment storage in a gravel-bed river. *Journal of Geophysical Research: Earth*
3
4 836 *Surface* **118**(2): 759–779. DOI: 10.1002/jgrf.20060.
5
6
7 837 Wheaton JM, Brasington J, Darby SE, Merz J, Pasternack GB, Sear D, Vericat D.
8
9 838 2010a. Linking geomorphic changes to salmonid habitat at a scale relevant to fish.
10
11 839 *River Research and Applications* **26**: 469–486. DOI: 10.1002/rra.
12
13
14 840 Wheaton JM, Brasington J, Darby SE, Sear DA. 2010b. Accounting for uncertainty in
15
16 841 DEMs from repeat topographic surveys: improved sediment budgets. *Earth Surface*
17
18 842 *Processes and Landforms* **35**: 136–156. DOI: 10.1002/esp.1886.
19
20
21
22 843 Williams RD, Brasington J, Hicks M, Measures R, Rennie CD, Vericat D. 2013.
23
24 844 Hydraulic validation of two-dimensional simulations of braided river flow with spatially
25
26 845 continuous aDcp data. *Water Resources Research* **49**(9): 5183–5205. DOI:
27
28 846 10.1002/wrcr.20391.
29
30
31
32 847 Williams RD, Brasington J, Vericat D, Hicks DM. 2014. Hyperscale terrain modelling
33
34 848 of braided rivers: fusing mobile terrestrial laser scanning and optical bathymetric
35
36 849 mapping. *Earth Surface Processes and Landforms* **39**(2): 167–183. DOI:
37
38 850 10.1002/esp.3437.
39
40
41
42 851 Woodget AS, Carbonneau PE, Visser F, Maddock IP. 2014. Quantifying submerged
43
44 852 fluvial topography using hyperspatial resolution UAS imagery and structure from
45
46 853 motion photogrammetry. *Earth Surface Processes and Landforms* **64**: 47–64. DOI:
47
48 854 10.1002/esp.3613.
49
50
51
52
53 855
54
55
56
57
58
59
60

Table 1. Main parameters for each flight performed and the average point density of the point clouds obtained. Note that the pixel resolution is the optimum established by the software according to image quality.

Model	Number of images	Average flight altitude <i>m</i>	Average pixel resolution <i>cm²/pix</i>	Average point density <i>p/m²</i>
October 2014	500	13.1	0.0556	1790
January 2015	361	15.6	0.0729	1370
April 2015	475	12.4	0.0454	2210

Table 2. Registration errors and model precision and accuracy of the October 2014, January 2015 and April 2015 point clouds. *Errors of the Ground Control Points (GCP) after georeferencing the point cloud. **Precision assessed as the standard deviation of the Check Point (ChP) residuals. ***Accuracy estimated as the mean value of the ChP residuals.

Model	Registration error* (m)				Model precision** (m)				Model accuracy*** (m)			
	x	y	z	3D	x	y	z	3D	x	y	z	3D
October 2014	0.031	0.030	0.021	0.050	0.031	0.031	0.022	0.025	0.025	0.024	0.014	0.044
January 2015	0.028	0.048	0.020	0.060	0.032	0.049	0.020	0.030	0.028	0.039	0.015	0.056
April 2015	0.030	0.019	0.011	0.039	0.031	0.020	0.012	0.017	0.025	0.016	0.009	0.035

1
2 865 Table 3. Volumetric changes extracted from the two thresholded DoD presented in
3
4 866 Figure 5. Two levels of thresholding have been applied, using statistical minLoD with
5
6
7 867 two t-scores ($t>1.28$ and $t>1.96$; 80% and 95% Confidence Interval respectively, see
8
9 868 text for more details).

	Minimum Level of Detection					
	80% CI ($t>1.28$)			95% CI ($t>1.96$)		
	Erosion	Deposition	Net change	Erosion	Deposition	Net change
	m^3	m^3	m^3	m^3	m^3	m^3
October 2014 - January 2015	-47.56	18.17	-29.39	-40.31	14.42	-25.88
January 2015 - April 2015	-158.19	34.80	-123.38	-146.21	30.36	-115.85

Figure 1. (A) Location of the study site (River Ehen, Lake District, NW England); (B) Original and new course of Ben Gill, from the old diversion to its confluence with the Ehen (point “P” shows position and direction of photograph in C); (C) Photograph of the newly created Ben Gill channel before reconnection (credit: EA Penrith).

Figure 2: Timing of the aerial photography surveys in relation to discharge measured at the River Ehen Bleach Green gauging station, approximately 800m downstream from the confluence of Ben Gill and the Ehen.

Figure 3. Schematic to illustrate the general workflow presented in this paper, including: (A) Preparation & experimentation, (B) Data collection, (C) Structure-from-Motion photogrammetry process preparation and (D) development, (E) Post-processing of outputs and (F) Production of results. Timeline runs through from A to F. Note that the abbreviations mean: ¹Ground Control Points, ²Structure-from-Motion Photogrammetry, ³Point Cloud, ⁴minimum Level of Detection, ⁵Digital Elevation Model.

Figure 4. Illustration of some workflow outputs: (A) An example of high resolution orthophoto (0.025m resolution) produced from the mosaic of individual images, (B) Result of the image classification process of the orthophotos, and (C) Digital Elevation Model (0.05m resolution). All relate to images taken in April 2015.

*Note that “Unclassified” in C refers to obstructing features that were not classified as sediments or vegetation (e.g. fences).

Figure 5. An example of roughness map (October 2014) of Ben Gill, with close-ups illustrating differences in roughness characteristics at various points along the channel. Roughness was estimated as the detrended standard deviation of the

1
2 896 elevations (see text for more details). Aerial photos are presented as a reference and
3
4 897 to help interpret roughness values.
5
6 898
7
8
9 899 Figure 6. Example of DEMs of Difference (DoD) of Ben Gill. DoDs were thresholded
10
11 900 using a minLoD (see text for more details): (A) October 2014-January 2015; (B)
12
13 901 January 2015-April 2015. Note that raster cells with topographic changes below the
14
15 902 minLoD are not coloured.
16
17 903
18
19
20
21 904 Figure 7. (A) Longitudinal profiles of Ben Gill thalweg extracted from the three
22
23 905 successive DEMs (from the top to the bottom of the newly created channel); (B) Close-
24
25 906 up of the downstream knick-point; (C) Close-up of the upstream knick-point. Black
26
27 907 arrows show the direction of knick-point migration.
28
29
30
31
32
33
34
35
36
37
38
39
40
41
42
43
44
45
46
47
48
49
50
51
52
53
54
55
56
57
58
59
60

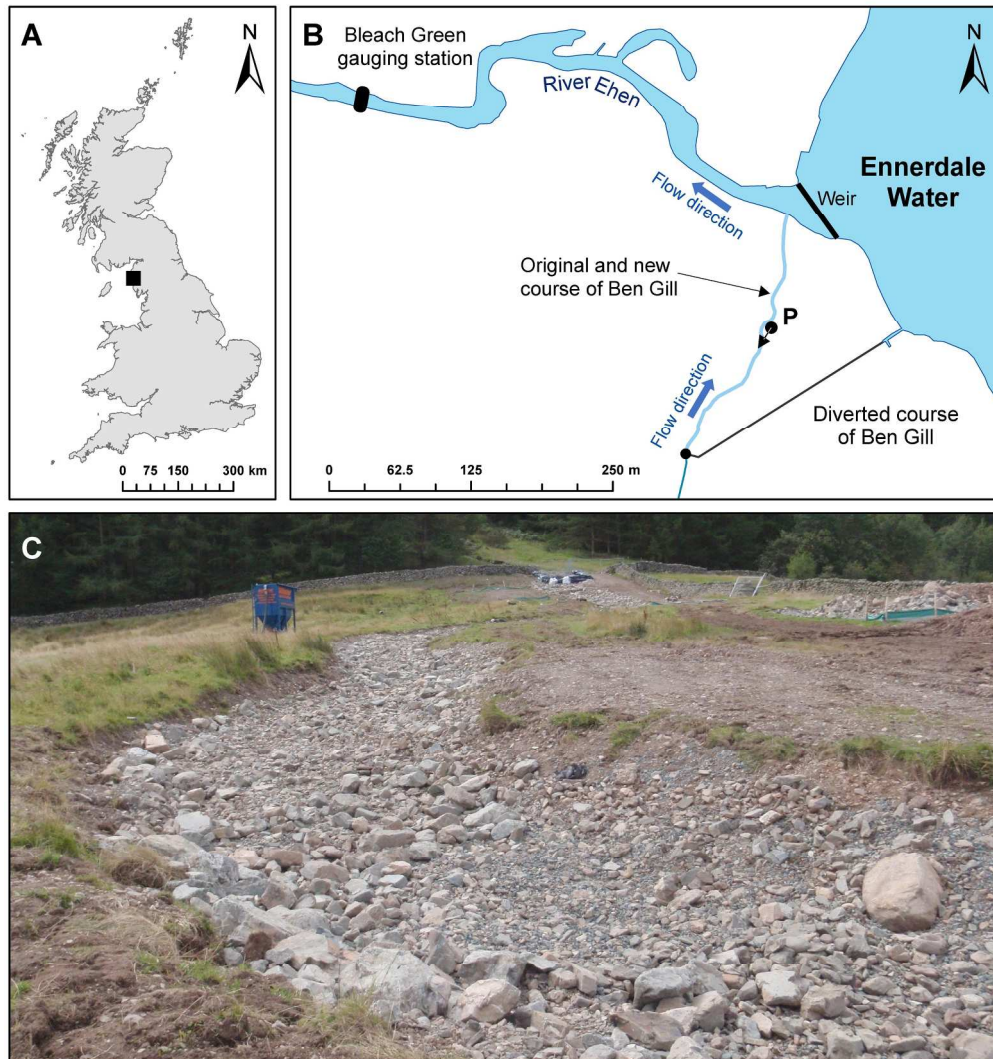


Figure 1. (A) Location of the study site (River Ehen, Lake District, NW England); (B) Original and new course of Ben Gill, from the old diversion to its confluence with the Ehen (point "P" shows position and direction of photograph in C); (C) Photograph of the newly created Ben Gill channel before reconnection (credit: EA Penrith).

Figure 1

224x240mm (300 x 300 DPI)

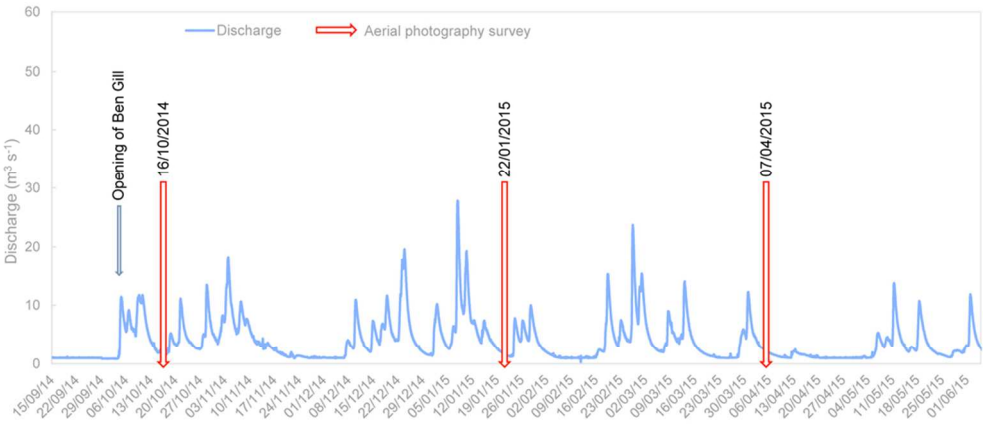


Figure 2: Timing of the aerial photography surveys in relation to discharge measured at the River Ehen Bleach Green gauging station, approximately 800m downstream from the confluence of Ben Gill and the Ehen.

Figure 2
90x39mm (300 x 300 DPI)

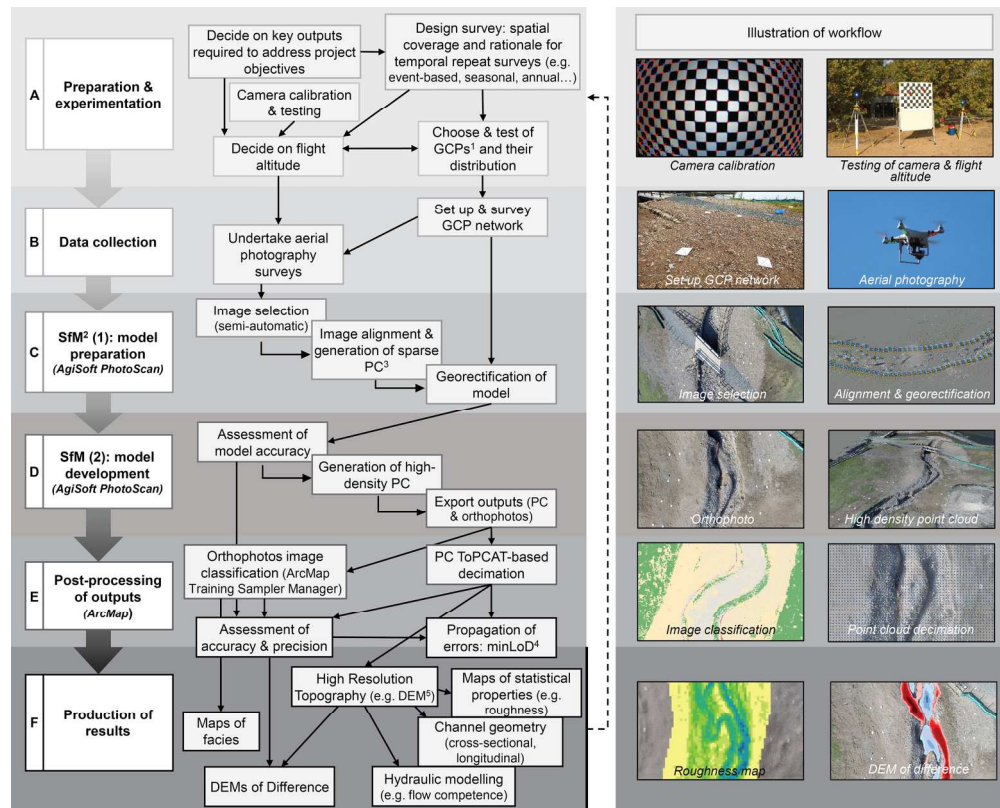


Figure 3. Schematic to illustrate the general workflow presented in this paper, including: (A) Preparation & experimentation, (B) Data collection, (C) Structure-from-Motion photogrammetry process preparation and (D) development, (E) Post-processing of outputs and (F) Production of results. Timeline runs through from A to F. Note that the abbreviations mean: 1Ground Control Points, 2Structure-from-Motion Photogrammetry, 3Point Cloud, 4minimum Level of Detection, 5Digital Elevation Model.

Figure 3

173x139mm (300 x 300 DPI)

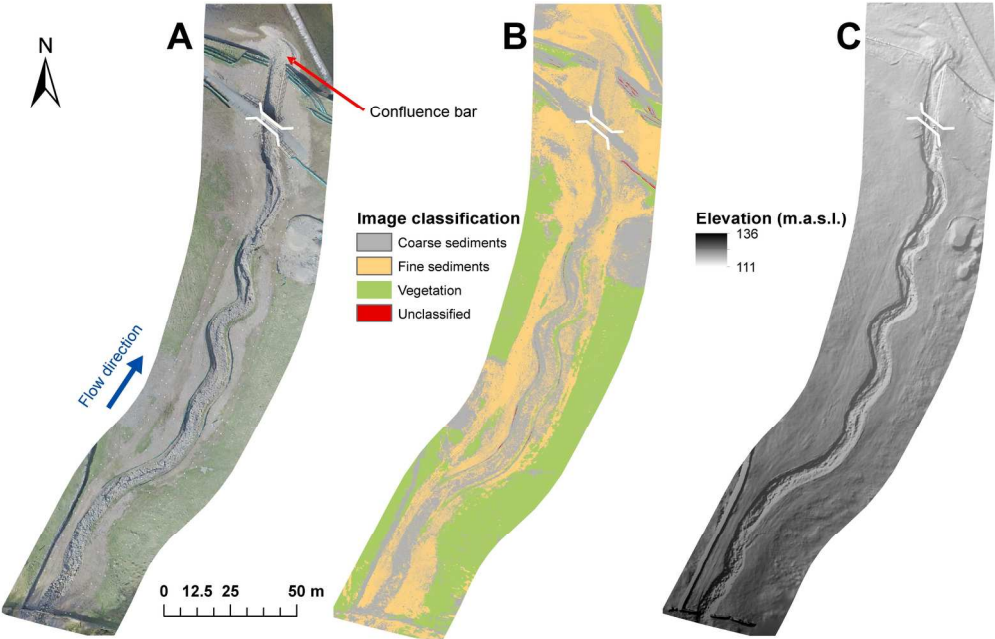


Figure 4. Illustration of some workflow outputs: (A) An example of high resolution orthophoto (0.025m resolution) produced from the mosaic of individual images, (B) Result of the image classification process of the orthophotos, and (C) Digital Elevation Model (0.05m resolution). All relate to images taken in April 2015. *Note that "Unclassified" in C refers to obstructing features that were not classified as sediments or vegetation (e.g. fences).

Figure 4
184x117mm (300 x 300 DPI)

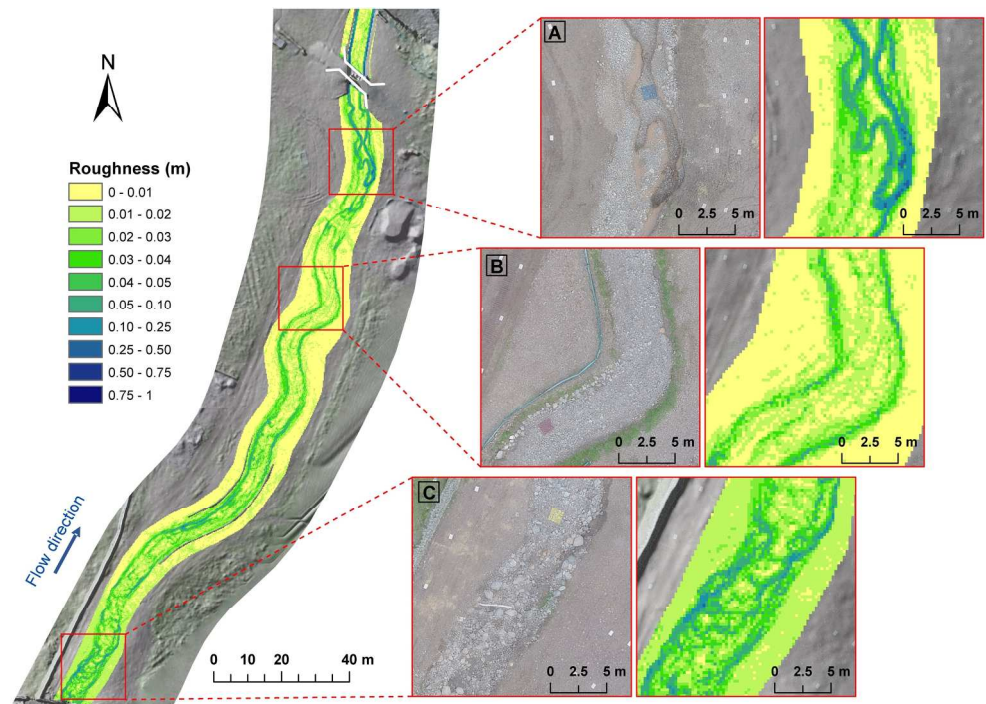


Figure 5. An example of roughness map (October 2014) of Ben Gill, with close-ups illustrating differences in roughness characteristics at various points along the channel. Roughness was estimated as the detrended standard deviation of the elevations (see text for more details). Aerial photos are presented as a reference and to help interpret roughness values.

Figure 5
207x145mm (300 x 300 DPI)

1
2
3
4
5
6
7
8
9
10
11
12
13
14
15
16
17
18
19
20
21
22
23
24
25
26
27
28
29
30
31
32
33
34
35
36
37
38
39
40
41
42
43
44
45
46
47
48
49
50
51
52
53
54
55
56
57
58
59
60

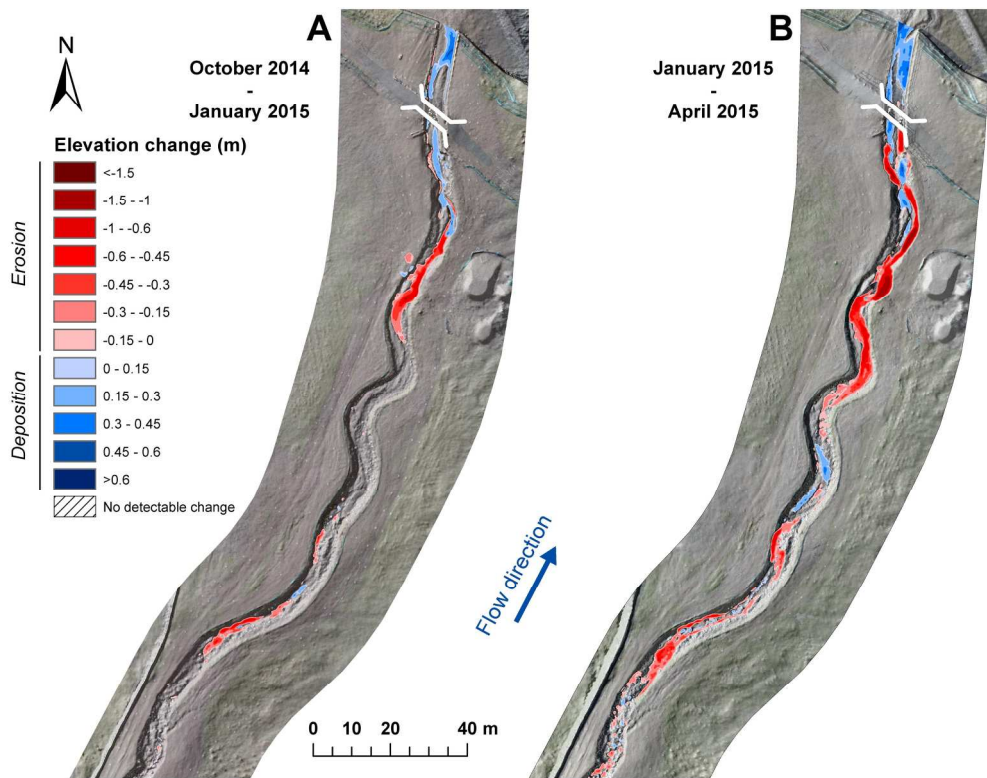


Figure 6. Example of DEMs of Difference (DoD) of Ben Gill. DoDs were thresholded using a minLoD (see text for more details): (A) October 2014-January 2015; (B) January 2015-April 2015. Note that raster cells with topographic changes below the minLoD are not coloured.

Figure 6
201x155mm (300 x 300 DPI)

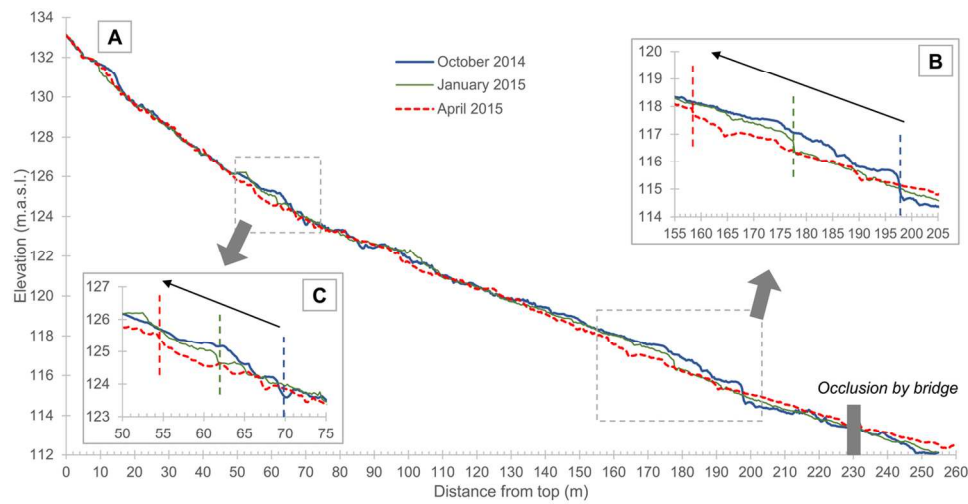


Figure 7. (A) Longitudinal profiles of Ben Gill thalweg extracted from the three successive DEMs (from the top to the bottom of the newly created channel); (B) Close-up of the downstream knick-point; (C) Close-up of the upstream knick-point. Black arrows show the direction of knick-point migration.

Figure 7

129x69mm (300 x 300 DPI)